Formation of a long-lived electron-transfer state of a naphthalene–quinolinium ion dyad and the π-dimer radical cation†

Hiroaki Kotani,[a] Kei Ohkubo[a] and Shunichi Fukuzumi*[ab]

Received 27th April 2011, Accepted 1st June 2011
DOI: 10.1039/c1fd00084e

An electron donor–quinolinium ion dyad, 2-phenyl-4-(1-naphthyl)quinolinium ion ($QuPh^+$–NA), has been synthesized based on a rational design. The X-ray crystal structure of $QuPh^+$–NA indicates that the dihedral angle between the NA and $QuPh^+$ moieties of $QuPh^+$–NA is nearly perpendicular. The one-electron reduction potential (E_{red}) was observed as a well-defined reversible wave at −0.90 V *versus* SCE. The one-electron reduced species ($QuPh^{\cdot}$–NA) was detected by ESR. The electron self-exchange rate constant (k_{ex}) between $QuPh^+$–NA and $QuPh^{\cdot}$–NA has been determined from the ESR linewidth alternation. The reorganization energy (λ) of the electron self-exchange was determined to be 0.42 eV from the k_{ex} value. Femtosecond laser irradiation of $QuPh^+$–NA at 355 nm results in formation of the ET state ($QuPh^{\cdot}$–$NA^{\cdot+}$) within 0.5 ps *via* photoinduced ET from NA to the singlet-excited state of $QuPh^+$. The transient absorption bands at 420 nm and 700 nm are assigned to the $QuPh^{\cdot}$ and $NA^{\cdot+}$ moieties, respectively. The nanosecond laser excitation of $QuPh^+$–NA affords the broad absorption band at 1000 nm and is due to the π-dimer radical cation formed between $QuPh^{\cdot}$–$NA^{\cdot+}$ and $QuPh^+$–NA. The intramolecular back electron-transfer process was too slow to compete with the intermolecular back electron-transfer reaction judging from the decay time profile of $QuPh^{\cdot}$–$NA^{\cdot+}$, which obeyed second-order kinetics.

Introduction

In the bacterial photosynthetic reaction center, sequential multi-step electron transfer (ET) occurs from the excited bacteriochlorophyll dimer [$(BChl)_2$] to the terminal electron acceptor *via* electron mediators to attain a long-lived charge-separated (CS) state.[1] Extensive efforts have so far been devoted to develop electron donor–acceptor linked multi-array systems, mimicking the photoinduced electron-transfer processes in the natural photosynthetic reaction center.[2–11] However, such a long-lived CS state has been attained in compensation for a significant energy loss during the multi-step ET processes, because each step loses a fraction of the initial excitation

[a]*Department of Material and Life Science, Graduate School of Engineering, Osaka University, ALCA, Japan Science and Technology Agency (JST), Suita, Osaka, 565-0871, Japan. E-mail: Fukuzumi@chem.eng.osaka.u.ac.jp; Fax: +81-6-6879-7370; Tel: +81-6-6879-7368*
[b]*Department of Bioinspired Science, Ewha Womans University, Seoul, 120-750, Korea*

† Electronic supplementary information (ESI) available: Fluorescence decay of quinolinium ion dyads (S1), cyclic voltammograms of $QuPh^+$–Ph (S2), ESR spectra of $QuPh^{\cdot}$–NA (S3), ESR spectrum of $QuPh^{\cdot}$–$NA^{\cdot+}$ at 77 K (S4), Transient absorption spectra of $QuPh^+$–NA with TCNB (S5), and X-ray Crystallographic data for $QuPh^+$–NA (Table S1). CCDC reference numbers 620443. For ESI and crystallographic data in CIF or other electronic format see DOI: 10.1039/c1fd00084e

energy with increases with the distance between the positive and negative charges. We have previously reported a much simpler approach to attain a high energy and long-lived ET state using closely linked molecular dyads based on rational design, which consists of two principles: (i) a short distance between electron donor and acceptor moieties to minimize the solvent reorganization energy (λ_s) of electron transfer (ET) and (ii) a choice of chromophore with a high-lying triplet excited state to attain the higher driving force ($-\Delta G_{bet}$) of back ET to the ground state rather than the triplet excited state.[11–20] Among them, the electron donor–acridinium ion dyad (*e.g.*, the 9-mesityl-10-methylacridinium ion), which has a small reorganization energy (λ) of ET because the overall charge remains the same in the charge-shift ET, is capable of fast photoinduced electron transfer but extremely slow back electron transfer to form a long-lived ET state and a π-dimer radical cation between the dyad and the ET state.[12] However, improvement of the reducing ability of the ET state is required for the more efficient photocatalytic production of hydrogen by the ET state. The quinolinium ion is a good candidate for such a purpose, because the one-electron reduction potential of the quinolinium ion is about 0.4 V more negative than that of the acridinium ion.[21]

We report herein the synthesis and X-ray crystal structure of the 2-phenyl-4-(1-naphthyl)quinolinium ion ($QuPh^+$–NA) in which the naphthalene (NA) donor moiety is directly linked with quinolinium ion (QuH^+) in comparison with the corresponding acridinium ion derivative (9-naphthyl-10-methylacridinium ion in Chart 1). The photophysical properties of $QuPh^+$–NA have been examined in detail in terms of formation of the ET state and the π-dimer radical cation as well as its reducing ability.

Results and discussion

Characterization of $QuPh^+$–NA

The synthetic procedure to make $QuPh^+$–NA, is slightly modified from the reported literature method,[22,23] and characterization is given in the Experimental Section. Recrystallization of $QuPh^+$–NA from methanol gave yellow crystals. The X-ray crystallographic analysis of $QuPh^+$–NA revealed that the dihedral angle was nearly perpendicular (87°) between the NA and Qu^+ moieties of $QuPh^+$–NA due to the steric interaction with the hydrogen at the *peri*-position as shown in Fig. 1a. This indicates that the orbital interaction between the NA and Qu^+ moieties is minimized, which was also supported by DFT calculations at the B3LYP/6-31G level (see Experimental Section) because the HOMO and LUMO orbitals of $QuPh^+$–NA were localized on the NA and Qu^+ moieties, respectively (Fig. 1b, c). The orthogonal geometry between the donor and acceptor moieties has also been reported for Acr^+–Mes.[12a]

The absorption spectrum of $QuPh^+$–NA (5.0×10^{-5} M) in acetonitrile (MeCN) shows characteristic absorption bands at 280 nm and 330 nm, which are assigned

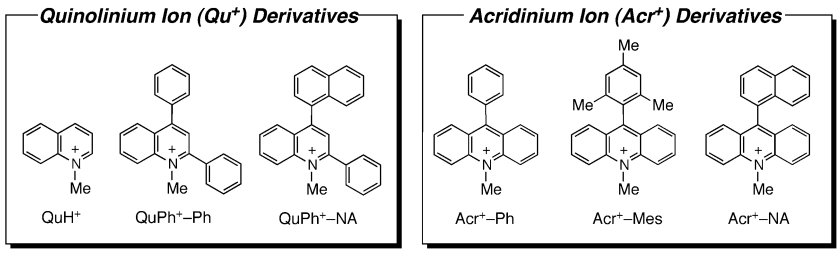

Chart 1 Chemical structures of electron-donor substituted quinolinium ions and acridinium ions.

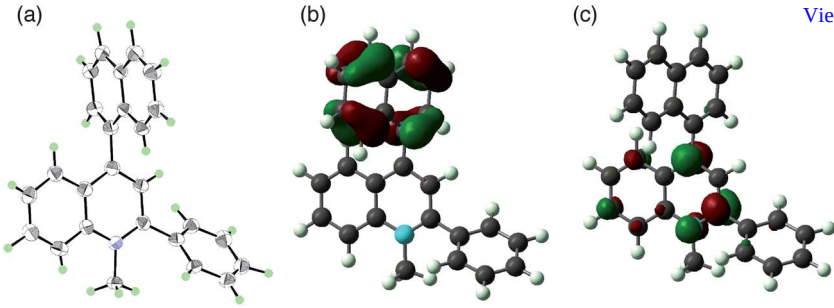

Fig. 1 (a) X-Ray crystal structure of $QuPh^+$–NA. (b) HOMO and (c) LUMO orbitals of $QuPh^+$–NA calculated by a DFT method (B3LYP/6-31G basis set).

to the NA and $QuPh^+$ moieties by comparison with the absorption spectra of naphthalene and 2,4-diphenylquinolinium ion (Fig. 2). $QuPh^+$–NA has an additional broad absorption band at 390 nm (3.18 eV), which is assigned to the charge-transfer (CT) transition from the NA to the $QuPh^+$ moiety,[24] because no such band is observed for the reference quinolinium ion ($QuPh^+$–Ph) in which the electron donor (NA) group is replaced by the phenyl (Ph) group (Fig. 2b).

The fluorescence spectrum of $QuPh^+$–NA is also shown in Fig. 2, together with that of $QuPh^+$–Ph at 298 K. $QuPh^+$–Ph emits strongly from the first singlet excited state of the quinolinium ion moiety ($^1QuPh^{+*}$: 3.53 eV)[25] with λ_{max} = 436 nm, whereas the emission from $^1QuPh^{+*}$ is totally quenched by the NA moiety in the case of $QuPh^+$–NA. Instead the emission from the singlet ET state of $QuPh^+$–NA in which an electron is transferred from the NA moiety to the $QuPh^+$ moiety, is observed at λ_{max} = 546 nm (2.27 eV) at 298 K. The lifetime of the ET emission of $QuPh^+$–NA and $QuPh^+$–Ph was determined to be 16 ns and 20 ns, respectively, which was similar to the fluorescence lifetime (20 ns) of $^1QuH^{+*}$ (see ESI†, Fig. S1). The absolute quantum yield of the ET emission of $QuPh^+$–NA was determined to be 15% (see Experimental Section).

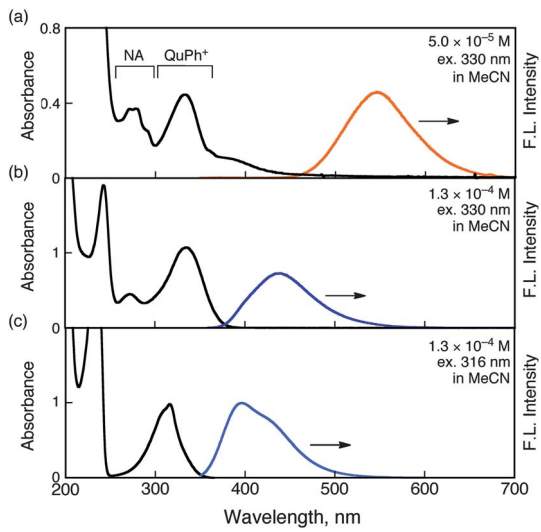

Fig. 2 UV-vis absorption spectra of (a) $QuPh^+$–NA and (b) $QuPh^+$–Ph and (c) Qu^+ in MeCN at 298 K. Fluorescence spectra of (a) $QuPh^+$–NA and (b) $QuPh^+$–Ph excited at 330 nm (c) QuH^+ excited at 316 nm in deaerated MeCN.

The one-electron oxidation (E_{ox}) and reduction (E_{red}) potentials of $QuPh^+$–NA were determined by cyclic voltammetry and second harmonic AC voltammetry (SHACV), respectively (Fig. 3). The one-electron reduction process of the $QuPh^+$ moiety is observed as a well-defined reversible wave at −0.90 V *versus* SCE because of the high stability of one-electron reduced species (Fig. 3b).[26,27] The redox potentials of $QuPh^+$–NA and $QuPh^+$–Ph are listed in Table 1 together with those of Acr^+–NA and Acr^+–Mes (ESI†, Fig. S2). The E_{red} value of the $QuPh^+$ moiety (−0.90 V) is much more negative that the E_{red} value of the Acr^+ moiety (−0.57 V),[28] indicating that the one-electron reduced species ($QuPh^{\cdot}$) is a much stronger reductant than $Acr^{\cdot}$. The driving force of photoinduced electron transfer ($-\Delta G_{ET}$) from the NA moiety to the singlet excited state of the $QuPh^+$ moiety and the back electron transfer ($-\Delta G_{BET}$) in MeCN were determined from the one-electron reduction potential and the excitation energy (3.53 eV) of the $QuPh^+$ moiety and the one-electron oxidation potential of the NA moiety. The $-\Delta G_{ET}$ and $-\Delta G_{BET}$ values are listed in Table 1 together with those of Acr^+–NA and Acr^+–Mes.[12c,28] The $-\Delta G_{BET}$ value of $QuPh^{\cdot}$–NA^{+} (2.77 eV) agrees with the singlet excited state energy of the ET state of $QuPh^+$–NA (2.73 eV), which is obtained as the average of the CT absorption (3.18 eV) and the ET emission (2.27 eV) in Fig. 2a.

ESR detection of $QuPh^{\cdot}$–NA and the electron-transfer self-exchange reaction

The fundamental electron-transfer properties of the quinolinium ion moiety of $QuPh^+$–NA were evaluated by the determination of the electron-transfer self-exchange reaction between $QuPh^{\cdot}$–NA and $QuPh^+$–NA. The $QuPh^{\cdot}$–NA was produced by visible light irradiation of a deaerated MeCN solution containing $QuPh^+$–NA and 1-benzyl-1,4-dihydronicotinamide dimer $(BNA)_2$,[29] which results in photoinduced electron transfer from $(BNA)_2$ to $QuPh^+$–NA to produce two equivalents of $QuPh^{\cdot}$–NA and BNA^+ [eqn (1)]. The UV-vis spectral change observed in the photochemical reduction of $QuPh^+$–NA (1.3×10^{-4} M) with $(BNA)_2$ (7.0×10^{-5} M) in deaerated MeCN is shown in Fig. 4, where new absorption bands at 420 nm and 510 nm are assigned to $QuPh^{\cdot}$–NA.

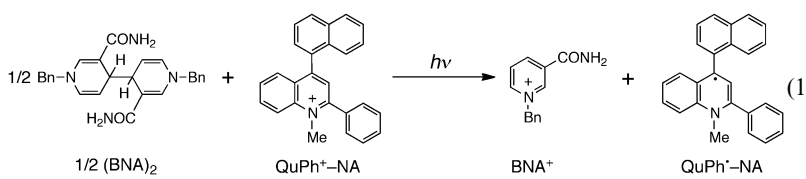

The produced $QuPh^{\cdot}$–NA is stable because of the steric hindrance caused by the NA group and it is readily detected by ESR in deaerated MeCN at 298 K as shown in Fig. 5a. The hyperfine splitting constants and the maximum slope linewidth (ΔH_{msl}) were determined by comparison of the observed spectrum with the computer-simulated spectrum shown in Fig. 5. The unpaired electron is delocalized

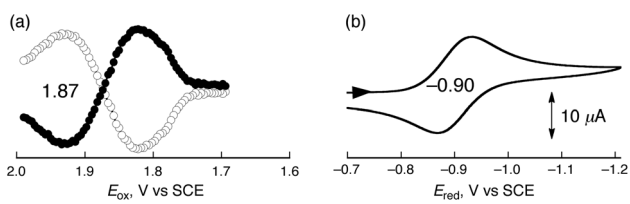

Fig. 3 (a) SHACV and (b) cyclic voltammogram of $QuPh^+$–NA (1.0×10^{-3} M) in deaerated MeCN containing TBAP (0.1 M) at 298 K; sweep rate;100 mV s^{-1}.

Table 1 One-electron oxidation potential (E_{ox} *versus* SCE), reduction potential (E_{red} *versus* SCE), driving force of photoinduced electron transfer ($-\Delta G_{ET}$) and back electron transfer ($-\Delta G_{BET}$) in MeCN at 298 K

Compound	E_{ox}/V	E_{red}/V	$-\Delta G_{ET}$/eV	$-\Delta G_{BET}$/eV
$QuPh^+$–Ph	[a]	−0.89		
$QuPh^+$–NA	1.87	−0.90	0.76	2.77
Acr^+–NA[b]	1.72	−0.55	0.50	2.27
Acr^+–Mes[c]	2.06	−0.57	0.26	2.63

[a] No oxidation wave was observed. [b] Ref. 12*c*. [c] Ref. 28.

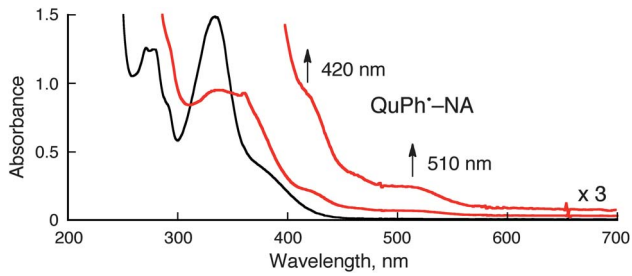

Fig. 4 UV-vis absorption spectra observed in the photochemical reduction of $QuPh^+$–NA (1.3×10^{-4} M) with $(BNA)_2$ (7.0×10^{-5} M) in deaerated MeCN after irradiation of visible light ($\lambda >$ 340 nm) at 298 K.

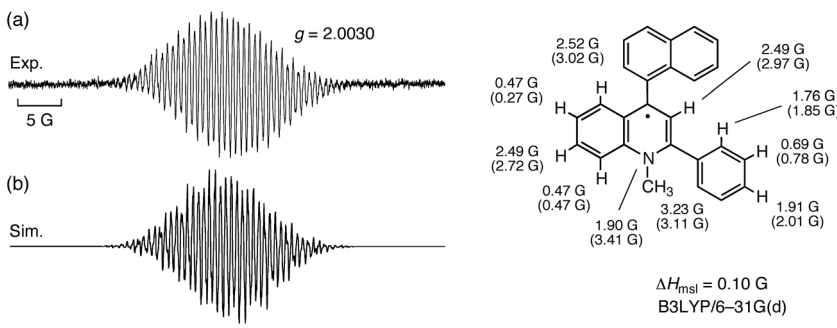

Fig. 5 (a) ESR spectrum of $QuPh^{\cdot}$–NA produced by the photochemical reduction of $QuPh^+$–NA (1.3×10^{-4} M) with $(BNA)_2$ (7.0×10^{-5} M) in deaerated MeCN at 298 K. (b) The simulated spectrum of $QuPh^{\cdot}$–NA using hyperfine coupling constants. The predicted values by DFT were shown in parentheses.

on the QuPh moiety as expected from the DFT calculation of the LUMO orbital in Fig. 1c. To determine the electron-transfer self-exchange rate constant (k_{ex}) between $QuPh^+$–NA and $QuPh^{\cdot}$–NA, ESR spectra of $QuPh^{\cdot}$–NA were measured in the presence of various concentrations of $QuPh^+$–NA in MeCN (ESI†, Fig. S3). The maximum slope linewidth (ΔH_{msl}) of each line increases linearly with an increase in concentration of $QuPh^+$–NA as shown in Fig. 6. The rate constant (k_{ex}) of the electron-transfer self-exchange reaction between $QuPh^+$–NA and $QuPh^{\cdot}$–NA was determined using eqn (2),[15a,30]

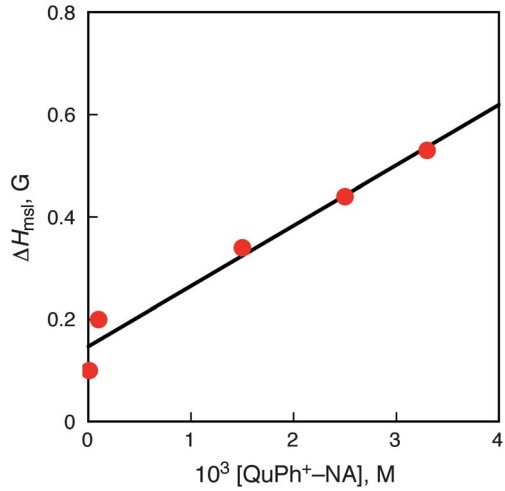

Fig. 6 Plot of ΔH_{msl} *versus* [QuPh$^+$–NA] for ESR spectra of QuPh$^{\cdot}$–NA in deaerated MeCN at 298 K.

$$k_{ex} = (1.52 \times 10^7)\,(\Delta H_{msl} - \Delta H^0_{msl})/\{(1 - P_i)[\text{QuPh}^+\text{–NA}]\} \quad (2)$$

where ΔH_{msl} and ΔH^0_{msl} are the maximum slope linewidths of the ESR spectra in the presence and absence of QuPh$^+$–NA, respectively, and P_i is a statistical factor, which can be taken as nearly zero. The k_{ex} value between QuPh$^{\cdot}$–NA and QuPh$^+$–NA determined to be 1.8×10^9 M^{-1} s^{-1}, which is smaller than the k_{ex} value between Acr$^{\cdot}$–Ph and Acr$^+$–Ph (3.1×10^9 M^{-1} s^{-1}).[30]

The reorganization energy (λ) of the electron-transfer self-exchange reaction is determined from the k_{ex} value using eqn (3), where k_{diff} is the diffusion rate constant in MeCN at 298 K (2.0×10^{10} M^{-1} s^{-1}) and Z is the collision frequency which is taken as 1×10^{11} M^{-1} s^{-1}.[15a,30] The λ value thus determined (0.40 eV) is larger than the value between Acr$^{\cdot}$–Ph and Acr$^+$–Ph (0.34 eV) because the delocalization of the electron in QuPh$^{\cdot}$–NA is less as compared to Acr$^{\cdot}$–Ph.

$$(k_{ex})^{-1} - (k_{diff})^{-1} = Z^{-1} \exp(\lambda/4kT) \quad (3)$$

Formation of the ET state of QuPh$^+$–NA

Femtosecond laser excitation at 390 nm of a deaerated MeCN solution of QuPh$^+$–NA (1.0×10^{-4} M) results in formation of the ET state (QuPh$^{\cdot}$–NA$^{\cdot+}$) within 0.5 ps, which has an absorption band at 420 nm due to QuPh$^{\cdot}$ and also at 690 nm due to NA$^{\cdot+}$,[31] as shown in Fig. 7a where the transient absorption spectrum of QuPh$^{\cdot}$–NA$^{\cdot+}$ is taken at 10 ps after laser excitation. The bleaching at 580 nm, which overlapps with the absorption due to QuPh$^{\cdot}$ (Fig. 7a), results from the CT emission in Fig. 2a. The CT emission results from the singlet ET state (QuPh$^{\cdot}$–NA). Time profiles of the transient absorption at 420 nm and 690 nm due to QuPh$^{\cdot}$–NA$^{\cdot+}$ are shown in Fig. 7b. In the time range, up to 1.5 ns, no decay of absorption at 690 nm due to QuPh$^{\cdot}$–NA$^{\cdot+}$ is observed. The slight increase in absorbance at 420 nm up to 1.5 ns in Fig. 7b may be ascribed to the recovery of the bleaching due to the CT absorption in Fig. 2a. The singlet ET state may be rapidly converted to the long-lived triplet ET state, which exhibits no decay up to 3 ns in contrast to the singlet ET state, which results in fluorescence with the lifetime of 16 ns (*vide supra*).

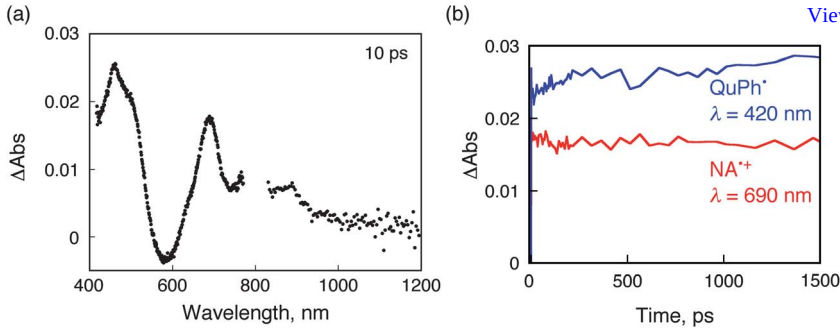

Fig. 7 (a) Transient absorption spectrum observed by the femtosecond laser excitation (λ = 390 nm) of a deaerated MeCN solution containing QuPh$^+$–NA (1.0×10^{-3} M) taken 10 ps after laser excitation at 295 K. (b) Decay time profiles at 420 nm due to QuPh$^\cdot$ and 690 nm due to NA$^{\cdot+}$.

The long-lived triplet ET state of QuPh$^+$–NA is observed by nanosecond laser excitation of a deaerated MeCN solution of QuPh$^+$–NA at 355 nm, which affords the same absorption spectrum due to the ET state as observed in Fig. 6 except for the newly formed absorption band at 1050 nm as shown in Fig. 8a.[12c,31] The NIR band at 1050 nm observed in Fig. 8a is well assigned due to the naphthalene π-dimer radical cation. Thus, the long-lived ET state (QuPh$^\cdot$–NA$^{\cdot+}$) forms the π-complex with QuPh$^+$–NA to afford the π-dimer radical cation (QuPh$^\cdot$–NA$^{\cdot+}$)(QuPh$^+$–NA), in which the NA$^{\cdot+}$ and QuPh$^\cdot$ moieties interact by π-bonding with the NA and QuPh$^+$ moieties, respectively.

The intramolecular back electron transfer in the π-dimer radical cation of the long-lived ET state was too slow to compete with the intermolecular (bimolecular) back electron transfer reaction between two π-dimer radical cations. In such a case, the decay of absorbance at 420 nm due to the QuPh$^\cdot$ moiety of the π-dimer radial cation obeyed second-order kinetics as shown in Fig. 8b. The rate constant of intermolecular back electron transfer was determined from the slope of the second-order plot and the molar absorption coefficient of QuPh$^\cdot$ at 420 nm (ε = 1500 M^{-1} cm^{-1}) to be 3.3×10^9 M^{-1} s^{-1}. The quantum yield of the π-dimer

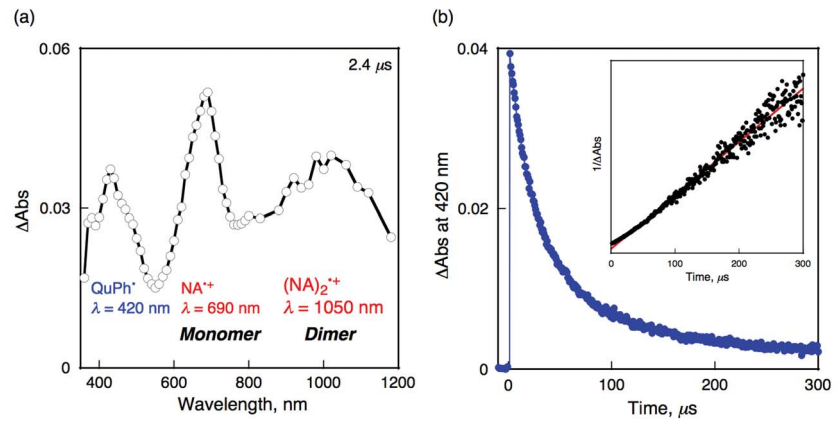

Fig. 8 (a) Transient absorption spectra of QuPh$^+$–NA (1.0×10^{-4} M) in deaerated MeCN at 298 K taken at 2.4 μs after laser excitation at 355 nm. (b) Decay time profile of absorbance at 420 nm due to QuPh$^\cdot$. Inset: second-order plot.

radical cation of the long-lived ET state of $QuPh^+$–NA was also determined by the comparative method to be 83%.[32] This value is consistent with the quantum yield of the ET emission (15%).

There has been discussion on the photoinduced state of Acr^+–NA (or Acr^+–Mes), which is either the ET state or the triplet excited state.[33] However, it has been demonstrated that the ET state is indeed produced, followed by formation of the π-dimer radical cation between Acr^+–Mes (or Acr^+–NA) and the ET state, which was also detected by NIR absorption due to the π–π^* transition of the π-dimer radical cation [(Acr^+–NA)($Acr^{\cdot}$–$NA^{\cdot+}$) or (Acr^+–Mes)($Acr^{\cdot}$–$Mes^{\cdot+}$)].[10c] In the case of $QuPh^+$–NA, the photoexcitation results in formation of the π-dimer radical cation between $QuPh^+$–NA and the ET state.

The formation of the triplet ET state was confirmed by ESR measurements.[15b,34] The typical triplet ESR signal ($g = 4.1$) was observed under photoirradiation of $QuPh^+$–NA (1.5×10^{-3} M) in deaerated MeCN at 77 K (see ESI†, Fig. S4).

Oxidizing and reducing abilities of the π-dimer radical cation of the ET state

In order to confirm the oxidizing ability of the π-dimer radical cation of the long-lived ET state of $QuPh^+$–NA, we examined the electron-transfer oxidation of 2-methoxynaphthalene (2-MeONA, $E_{ox} = 1.38$ V *versus* SCE) with $QuPh^{\cdot}$–$NA^{\cdot+}$. Nanosecond laser excitation of a deaerated MeCN solution of $QuPh^+$–NA containing 2-MeONA results in the formation of the 2-MeONA radical cation ($2\text{-MeONA}^{\cdot+}$; $\lambda_{max} = 520$, 600 nm), whereas the transient absorption due to $QuPh^{\cdot}$–NA ($\lambda_{max} = 420$ nm) remains the same as shown in Fig. 9a. The decay of absorption at 690 nm due to $NA^{\cdot+}$ obeyed pseudo-first-order kinetics and the pseudo-first-order rate constant increased linearly with [2-MeONA] as shown in Fig. 9b. The second-order rate constant (k_{et}) of electron transfer from $NA^{\cdot+}$ to 2-MeONA is determined from the slope of the linear plot in Fig. 9b to be 1.1×10^9 M^{-1} s^{-1}. This indicates that an exergonic electron transfer from 2-MeONA ($E_{ox} = 1.38$ V) to $QuPh^{\cdot}$–$NA^{\cdot+}$ ($E_{red} = 1.87$ V) occurs efficiently to produce $2\text{-MeONA}^{\cdot+}$ and $QuPh^{\cdot}$–NA.

The reducing ability of the π-dimer radical cation of the long-lived ET state of $QuPh^+$–NA (E_{ox} of $QuPh^{\cdot}$–$NA^{\cdot+}$ *versus* SCE = −0.90 V) is expected to be stronger than that of Acr^+–Mes (E_{ox} of $Acr^{\cdot}$–Mes^+ *versus* SCE = −0.57 V).[28,35] The one-electron reduction of hexyl viologen (HV^{2+}) and tetracyanobenzene (TCNB) with $QuPh^{\cdot}$–$NA^{\cdot+}$ and $Acr^{\cdot}$–$Mes^{\cdot+}$ was examined in detail. In the case of HV^{2+} ($E_{red} = -0.42$ V),[36a] the transient absorption bands at 400 nm and 600 nm due to $HV^{\cdot+}$ were observed *via* intermolecular ET from the $QuPh^{\cdot}$ moiety to HV^{2+} in

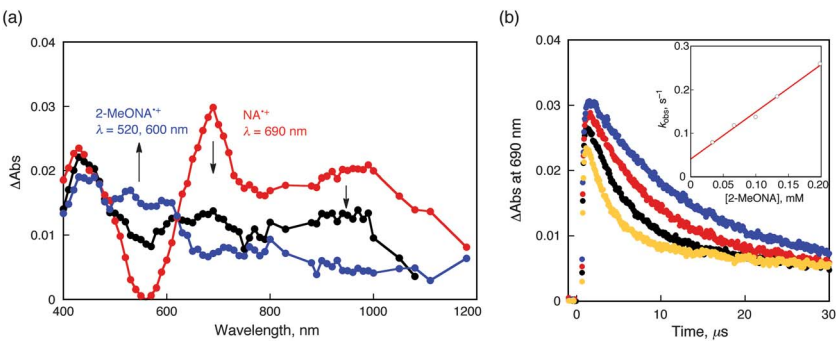

Fig. 9 (a) Transient absorption spectra of $QuPh^+$–NA (1.0×10^{-4} M) with 2-MeONA (2.6×10^{-4} M) in deaerated MeCN at 298 K taken at 2.4 μs after laser excitation at 355 nm. (b) Decay time profiles at 690 nm due to $NA^{\cdot+}$ in the presence of 2-MeONA (3.0×10^{-5}–2.0×10^{-4} M) in deaerated MeCN containing $QuPh^+$–NA (1.0×10^{-4} M). Inset: plot of the pseudo-first-order decay rate constant *versus* [2-MeONA].

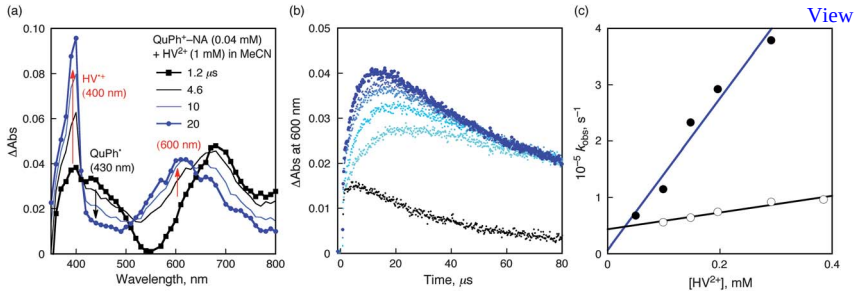

Fig. 10 (a) Transient absorption spectra of $QuPh^+$–NA (1.0×10^{-4} M) with HV^{2+} (1.0×10^{-3} M) in deaerated MeCN at 298 K taken at 2.4 μs after laser excitation at 355 nm. (b) Absorbance time profiles at 600 nm due to $HV^{\bullet+}$ in the presence of various concentration of HV^{2+}. (c) Plot of the pseudo-first-order rate constant (k_{obs}) for electron transfer from $QuPh^{\bullet}$–$NA^{\bullet+}$ to HV^{2+} *versus* $[HV^{2+}]$ (black circles: ●). Plot of k_{obs} *versus* $[HV^{\bullet+}]$ for electron transfer from $Acr^{\bullet}$–$Mes^{\bullet+}$ to $HV^{\bullet+}$ is shown as open circles (○).

Fig. 10a. The ET rates obeyed pseudo-first-order kinetics and the observed pseudo-first-order rate constant (k_{obs}) increased linearly with increasing concentration of HV^{2+} as shown in Fig. 10b. The ET rate constant (k_{et}) was determined from the slope of the linear plot in Fig. 10b to be 1.3×10^9 M^{-1} s^{-1} (●), which is much larger than the k_{et} value of $Acr^{\bullet}$–$Mes^{\bullet+}$ (1.0×10^8 M^{-1} s^{-1}, ○). When HV^{2+} is replaced by TCNB ($E_{red} = -0.74$ V),[35,36b] ET from the $QuPh^{\bullet}$ moiety to TCNB occurred efficiently, although no ET was observed in the case of Acr^+–Mes, because the free energy change of ET from $Acr^{\bullet}$ to TCNB is endergonic ($\Delta G_{et} = 0.17$ eV) as shown in Fig. S5 (ESI†). Thus, it has been confirmed that the π-dimer radical cation of long-lived ET state of $QuPh^+$–NA has a much stronger reducing ability than that of Acr^+–Mes.

Conclusion

In conclusion, we have designed and synthesized a naphthalene–quinolinium ion dyad ($QuPh^+$–NA) to achieve the formation of a long-lived ET state on the basis of rational design. Photoirradiation of $QuPh^+$–NA results in the formation of the long-lived ET state together with the π-dimer radical cation between $QuPh^{\bullet}$–$NA^{\bullet+}$ and $QuPh^+$–NA. The reducing ability of the π-dimer radical cation of the long-lived ET state has been much improved in comparison with that of $Acr^{\bullet}$–$Mes^{\bullet+}$. Thus, $QuPh^+$–NA is expected to act as a more efficient photocatalyst for the catalytic production of hydrogen in terms of electron injection to metal nanoparticles, which is now in progress.[37]

Experimental

General procedures

All of the reagents used in the syntheses, obtained from Aldrich Chemicals and Tokyo Chemical Industry Co., Ltd. were the best available purity and used without further purification. ^{1}H NMR spectra (300 MHz) were recorded on a JEOL AL-300 spectrometer at 298 K and chemical shifts (ppm) were determined relative to residual solvent peaks. MALDI-TOF-MS measurements were performed on a Kratos Compact MALDI I (Shimadzu) using dithranol as a matrix. UV-vis spectroscopy was carried out on a Hewlett Packard 8453 diode array spectrophotometer with a quartz cuvette (path length = 10 mm) at 298 K. Fluorescence measurements were performed on a Shimadzu RF-5300PC fluorescence spectrophotometer. The quantum yield of the ET emission was determined by using an absolute PL quantum

yield measurement system (Hamamatsu photonics Co., Ltd., C9920-02) with excitation at 430 nm.

Syntheses of 2,4-substituted quinolinium ions

The 2,4-substituted quinolinium ions were synthesized by following procedures as shown in Scheme 1.

1′-Naphtyl-2-aminobenzophenone (1). To a solution of anthranilic acid *N*-methoxy-*N*-methylamide[22] (2.00 g, 11.1 mmol) and 1-bromonaphthalene (2.29 g, 11.1 mmol) in anhydrous THF (60 mL) at −78 °C was added, with vigorous stirring, *n*-BuLi in hexanes (13.8 mL, 1.6 M, 22.2 mmol) over 20 min. After the dropwise addition, HCl (1 N, 20 mL) was added, and the mixture was extracted with ethyl acetate (150 mL) and washed with water (2 × 100 mL) and brine (50 mL). The organic layer was evaporated and purified by column choromatography with $CHCl_3$ to afford **1** as a red oil (500 mg, 18%): ^{1}H NMR (300 MHz, $CDCl_3$) δ 7.97–7.93 (m, 3H), 7.49–7.42 (m, 4H), 7.28–7.20 (m, 2H), 6.73 (d, J = 7.5 Hz, 1H), 6.52 (bs, 1H), 6.43 (t, J = 7.5 Hz, 3H).

2-Phenyl-4-(1-naphtyl)quinoline (2). **1** (400 mg, 1.6 mmol) and acetophenone (400 mg, 4.4 mmol) were added along with diphenyl phosphate (2.5 g, 10.0 mmol) and *m*-cresol (1.6 g, 14.8 mmol).[23] The reaction mixture was purged with argon and stirred at 140 °C for 5 h. After cooling, dichloromethane (100 mL) and 10% NaOH (100 mL) were added to the reaction mixture. The organic layer was separated, washed with water (3 × 100 mL) and brine (50 mL) and evaporated. The crude product was purified by column choromatography eluted with $CHCl_3$ to give **2** as a pale-yellow solid (150 mg, 28%). ^{1}H NMR (300 MHz, $CDCl_3$) δ 8.27 (d, J = 8.5 Hz, 1H), 8.21 (d, J = 8.5 Hz, 2H), 7.97 (t, J = 8.5 Hz, 2H), 7.91 (s, 1H), 7.71 (t, J = 8.5 Hz, 1H), 7.61–7.32 (m, 11H).

2-Phenyl-4-(1-naphtyl)quinolinium perchlorate (QuPh$^+$–NA). A solution of **2** (150 mg, 0.45 mmol) in dichloromethane (10 mL) was treated with methyl triflate (82 mg, 0.50 mmol). The reaction mixture was stirred at room temperature for 2 h. After removal of the solvent, the residue was stirred in MeOH (20 mL) and then $NaClO_4$ (0.12 g, 1.0 mmol) was added to the solution. The solution was evaporated and subsequent recrystallization from MeOH gave QuPh$^+$–NA as a yellow solid (190 mg, 95%): ^{1}H NMR (300 MHz, CD_3CN) δ 8.52 (d, J = 9.0 Hz, 1H), 8.25 (t, J = 9.0 Hz, 1H), 8.18 (d, J = 9.0 Hz, 1H), 8.08 (d, J = 9.0 Hz, 1H), 8.05 (s, 1H), 7.82–7.69 (m, 8H), 7.61 (t, J = 9.0 Hz, 2H), 7.45 (t, J = 9.0 Hz, 1H), 7.41 (d, J = 9.0 Hz, 1H), 4.44 (s, 3H), MALDI-TOF-MS m/z 346 (M^+ calcd for $C_{20}H_{16}N$ 346.2). Anal. calcd for $C_{26}H_{20}ClNO_4$: C, 70.03; H, 4.52; N, 3.14. Found: C, 69.78; H, 4.39; N, 3.19.

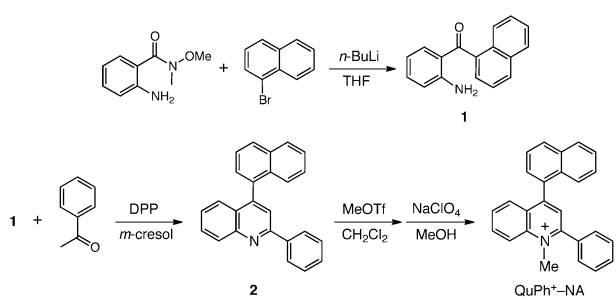

Scheme 1

2,4-Diphenylquinolinium perchlorate (QuPh$^+$–Ph). The 1′-naphtyl-2-aminobenzophenone (400 mg, 1.6 mmol) used in synthesis of QuPh$^+$–Ph was replaced by 2-aminobenzophenone (400 mg, 2.0 mmol). QuPh$^+$–Ph was isolated as a white solid (150 mg, 19%): ^{1}H NMR (300 MHz, CD_3CN) δ 8.48 (d, J = 8.4 Hz, 1H), 8.31–8.25 (m, 2H), 7.98 (t, J = 8.4 Hz, 1H), 7.95 (s, 1H), 7.75–7.67 (m, 10H), 4.36 (s, 3H), MALDI-TOF-MS *m/z* 270 (M^+ calcd for $C_{20}H_{16}N$ 270.1).

X-Ray crystallographic analysis

Crystallographic data for QuPh$^+$–NA has been deposited with the Cambridge Crystallographic Data Center as supplementary publication No. CCDC-620443. Copies of the data can be obtained free of charge on application to the CCDC, 12 Union Road, Cambridge CB21EZ, U.K. (fax, (+44)-1223-336-033; e-mail, deposit@ccdc.cam.ac.uk). Measurements were made on a Rigaku/MSC Mercury CCD diffractometer with graphite-monochromated Mo-Kα radiation (λ = 0.7107 Å). Data were collected and processed using the CrystalClear program (Rigaku). Crystallographic data. All data were refined anisotropically by the full-matrix least-squares method on F^2 for non-hydrogen atoms (SHELXL-97).[38] Crystallographic data was summarized in Table S1 (ESI†).

Electrochemical measurements

Cyclic voltammetry (CV) measurements were performed at 298 K on an ALS630B electrochemical analyzer in deaerated acetonitrile (MeCN) containing 0.1 M Bu_4NClO_4 (TBAP) as the supporting electrolyte. A conventional three-electrode cell was used with a platinum working electrode (surface area of 0.3 mm^2) and a platinum wire as the counter electrode. The Pt working electrode (BAS) was routinely polished with a BAS polishing alumina suspension and rinsed with acetone before use. The second harmonic AC voltammetry (SHACV)[39] measurements were performed on an ALS630B electrochemical analyzer. The measured potentials were recorded with respect to the $Ag/AgNO_3$ (0.01 M) reference electrode. The redox potentials (*versus* Ag/Ag^+) are converted to those *versus* SCE by adding 0.29 V.[40] All electrochemical measurements were carried out under an atmospheric pressure of argon.

Time-resolved absorption measurements

Ultrafast transient absorption spectroscopy experiments were conducted using an ultrafast source: Integra-C (Quantronix Corp.), an optical parametric amplifier: TOPAS (Light Conversion Ltd.) and a commercially available optical detection system: Helios provided by Ultrafast Systems LLC. The source for the pump and probe pulses were derived from the fundamental output of Integra-C (780 nm, 2 mJ/pulse and fwhm = 130 fs) at a repetition rate of 1 kHz. 75% of the fundamental output of the laser was introduced into TOPAS which has optical frequency mixers resulting in a tunable range from 285 nm to 1660 nm, while the rest of the output was used for white light generation. Prior to generating the probe continuum, a variable neutral density filter was inserted in the path in order to generate stable continuum, then the laser pulse was fed to a delay line that provides an experimental time window of 3.2 ns with a maximum step resolution of 7 fs. In our experiments, a wavelength between 350 nm to 450 nm of TOPAS output, which are the fourth harmonic of signal or idler pulses, was chosen as the pump beam. As this TOPAS output consists of not only desirable wavelength but also unnecessary wavelengths, the latter was deviated using a wedge prism with a wedge angle of 18 degree. The desirable beam was irradiated at the sample cell with a spot size of 1 mm diameter where it was merged with the white probe pulse in a close angle (<10 degree). The probe beam after passing through the 2 mm sample cell was focused on a fiber optic cable, which was connected to a CCD spectrograph for recording the time-resolved spectra

(410–800 nm). Typically, 2500 excitation pulses were averaged for 5 s to obtain the transient spectrum at a set delay time. Kinetic traces at appropriate wavelengths were assembled from the time-resolved spectral data. All measurements were conducted at room temperature, 295 K.

For nanosecond laser flash photolysis experiments, a deaerated MeCN solution of $QuPh^+$–NA were excited by an Nd:YAG laser (Continuum, SLII-10, 4–6 ns fwhm) at $\lambda = 355$ nm with the power of 10 mJ per pulse. The transient absorption measurements in the visible and near-IR region were performed using a continuous xenon lamp (150 W) as a probe light and a photomultiplier (Hamamatsu R2949; 350–800 nm) and an InGaAs-PIN photodiode (Hamamatsu G5125–10; 800–1200 nm) as a detector, respectively. The output from the photodiodes and a photomultiplier was recorded with a digitizing oscilloscope (Tektronix, TDS3032, 300 MHz).

ESR measurements

The ESR spectra were taken on a JEOL X-band spectrometer (JES-RE1XE) with a quartz ESR tube (1.2 mm i.d.) at 298 K. A deaerated MeCN solution containing $(BNA)_2$ (2.0×10^{-4} M) and $QuPh^+$–NA (1.0×10^{-4} M) was irradiated with a high-pressure mercury lamp (USH–1005D) through a water filter focusing at the sample cell in the ESR cavity. Simulations of ESR signals were made by using a WinSIM program[41] to determine the hyperfine coupling constants and maximum slope linewidths.

Theoretical calculations

Density-functional theory (DFT) calculations were performed on an 8CPU workstation (PQS, Quantum Cube QS8-2400C-064). Geometry optimizations were carried out using the Becke3LYP functional and 6-31G basis set[42,43] for the ground state of $QuPh^+$–NA and Becke3LYP functional and 6-31G(d) basis set for the quinolinyl radical ($QuPh^{\cdot}$–NA) with the unrestricted Hartree–Fock (UHF) formalism and as implemented in the Gaussian 03 program Revision C.02. Graphical outputs of the computational results were generated with the Gauss View software program (ver. 3.09) developed by Semichem, Inc.

Acknowledgements

This work was supported by a Grant-in-Aid (No. 20108010 and 23750014) and the Global COE (center of excellence) program "Global Education and Research Center for Bio-Environmental Chemistry" of Osaka University from the Ministry of Education, Culture, Sports, Science and Technology, Japan, KOSEF/MEST through WCU project (R31-2008-000-10010-0) of Korea.

References

1 (*a*) *The Photosynthetic Reaction Center*, J. Deisenhofer and J. R. Norris, ed. Academic Press; San Diego, 1993; (*b*) *Molecular Level Artificial Photosynthetic Materials*, G. J. Meyer, Ed. Wiley, New York, 1997.
2 (*a*) D. Gust, T. A. Moore and A. L. Moore, *Acc. Chem. Res.*, 2001, **34**, 40; (*b*) D. Gust, T. A. Moore and A. L. Moore, In *Electron Transfer in Chemistry*, V. Balzani, Ed. Wiley, Weinheim, 2001, vol. 3, pp. 272–336; (*c*) M. N. Paddon-Row, *Acc. Chem. Res.*, 1994, **27**, 18; (*d*) D. Gust, T. A. Moore and A. L. Moore, *Acc. Chem. Res.*, 1993, **26**, 198; (*e*) D. Gust, T. A. Moore and A. L. Moore, *Acc. Chem. Res.*, 2009, **42**, 1890.
3 (*a*) M. R. Wasielewski, *Chem. Rev.*, 1992, **92**, 435; (*b*) K. D. Jordan and M. N. Paddon-Row, *Chem. Rev.*, 1992, **92**, 395; (*c*) F. D. Lewis, R. L. Letsinger and M. R. Wasielewski, *Acc. Chem. Res.*, 2001, **34**, 159; (*d*) M. R. Wasielewski, *Acc. Chem. Res.*, 2009, **42**, 1910.
4 (*a*) V. Balzani, P. Ceroni, A. Juris, M. Venturi, S. Campagna, F. Puntoriero and S. Serroni, *Coord. Chem. Rev.*, 2001, **219–221**, 545; (*b*) V. Balzani, A. Credi and M. Venturi, *ChemSusChem*, 2008, **1**, 26.

5 (*a*) M.-J. Blanco, M. C. Jiménez, J.-C. Chambron, V. Heitz, M. Linke and J.-P. Sauvage, *Chem. Soc. Rev.*, 1999, **28**, 293; (*b*) F. Diederich and M. Gómez-López, *Chem. Soc. Rev.*, 1999, **28**, 263; (*c*) A. Harriman and J.-P. Sauvage, *Chem. Soc. Rev.*, 1996, **25**, 41.
6 (*a*) S. Fukuzumi and D. M. Guldi, in *Electron Transfer in Chemistry*; V. Balzani, Ed. Wiley, Weinheim 2001, vol. 2. pp. 270–337; (*b*) S. Fukuzumi, *Org. Biomol. Chem.*, 2003, **1**, 609; (*c*) S. Fukuzumi, *Phys. Chem. Chem. Phys.*, 2008, **10**, 2283; (*d*) S. Fukuzumi, *Bull. Chem. Soc. Jpn.*, 2006, **79**, 177; (*e*) S. Fukuzumi and T. Kojima, *J. Mater. Chem.*, 2008, **18**, 1427.
7 (*a*) L. Flamigni, F. Barigelletti, N. Armaroli, J.-P. Collin, I. M. Dixon, J.-P. Sauvage and J. A. G. Williams, *Coord. Chem. Rev.*, 1999, **190–192**, 671; (*b*) M. Linke, J.-C. Chambron, V. Heitz, J.-P. Sauvage, S. Encinas, F. Barigelletti and L. Flamigni, *J. Am. Chem. Soc.*, 2000, **122**, 11834; (*c*) I. M. Dixon, J.-P. Collin, J.-P. Sauvage, F. Barigelletti and L. Flamigni, *Angew. Chem., Int. Ed.*, 2000, **39**, 1292.
8 (*a*) P. V. Kamat, *J. Phys. Chem. C*, 2007, **111**, 2834; (*b*) N. K. Subbaiyan, C. A. Wijesinghe and F. D'Souza, *J. Am. Chem. Soc.*, 2009, **131**, 14646; (*c*) H. Imahori, T. Umeyama and S. Ito, *Acc. Chem. Res.*, 2009, **42**, 1809.
9 (*a*) H. Imahori, K. Tamaki, D. M. Guldi, C. Luo, M. Fujitsuka, O. Ito, Y. Sakata and S. Fukuzumi, *J. Am. Chem. Soc.*, 2001, **123**, 2607; (*b*) H. Imahori, D. M. Guldi, K. Tamaki, Y. Yoshida, C. Luo, Y. Sakata and S. Fukuzumi, *J. Am. Chem. Soc.*, 2001, **123**, 6617.
10 (*a*) C. A. Wijesinghe, M. E. El-Khoury, N. K. Subbaiyan, M. Supur, M. E. Zandler, K. Ohkubo, S. Fukuzumi and F. D'Souza, *Chem.–Eur. J.*, 2011, **17**, 3147; (*b*) K. Ohkubo, P. J. Sintic, N. V. Tkachenko, H. Lemmetyinen, W. E. Z. Ou, J. Shao, K. M. Kadish, M. J. Crossley and S. Fukuzumi, *Chem. Phys.*, 2006, **326**, 3; (*c*) F. J. Cépedes-Guirao, K. Ohkubo, S. Fukuzumi, Á. Sastre-Santos and F. Fernández-Lázaro, *J. Org. Chem.*, 2009, **74**, 5871; (*d*) M. Murakami, K. Ohkubo, T. Hasobe, V. Sgobba, D. M. Guldi, F. Wessendorf, A. Hirsh and S. Fukuzumi, *J. Mater. Chem.*, 2010, **20**, 1457; (*e*) F. D'Souza, N. K. Subbaiyan, Y. Xie, J. P. Hill, K. Ariga, K. Ohkubo and S. Fukuzumi, *J. Am. Chem. Soc.*, 2009, **131**, 16138; (*f*) Á. J. Jiménez, F. Spänig, M. S. Rodríguez-Morgade, K. Ohkubo, S. Fukuzumi, D. M. Guldi and T. Torres, *Org. Lett.*, 2007, **9**, 2481; (*g*) L. Martín-Gomis, K. Ohkubo, F. Fernández-Lázaro, S. Fukuzumi and Á. Sastre-Santos, *Chem. Commun.*, 2010, **46**, 3944.
11 (*a*) K. Ohkubo and S. Fukuzumi, *Bull. Chem. Soc. Jpn.*, 2009, **82**, 303; (*b*) K. Ohkubo and S. Fukuzumi, *J. Porphyrins Phthalocyanines*, 2008, **12**, 993.
12 (*a*) S. Fukuzumi, H. Kotani, K. Ohkubo, S. Ogo, N. V. Tkachenko and H. Lemmetyinen, *J. Am. Chem. Soc.*, 2004, **126**, 1600; (*b*) K. Ohkubo, H. Kotani and S. Fukuzumi, *Chem. Commun.*, 2005, 4520; (*c*) S. Fukuzumi, H. Kotani and K. Ohkubo, *Phys. Chem. Chem. Phys.*, 2008, **10**, 5159; (*d*) N. Mizoshita, K. Yamanaka, T. Shimada, T. Tani and S. Inagaki, *Chem. Commun.*, 2010, **46**, 9235; (*e*) S. Zilberg, *Phys. Chem. Chem. Phys.*, 2010, **12**, 10292.
13 (*a*) S. Fukuzumi, K. Ohkubo, H. Imahori, J. Shao, Z. Ou, G. Zheng, Y. Chen, R. K. Pandey, M. Fujitsuka, O. Ito and K. M. Kadish, *J. Am. Chem. Soc.*, 2001, **123**, 10676; (*b*) K. Ohkubo, H. Imahori, J. Shao, Z. Ou, K. M. Kadish, Y. Chen, G. Zheng, R. K. Pandey, M. Fujitsuka, O. Ito and S. Fukuzumi, *J. Phys. Chem. A*, 2002, **106**, 10991.
14 F. D'Souza, E. Maligaspe, K. Ohkubo, M. E. Zandler, N. K. Subbaiyan and S. Fukuzumi, *J. Am. Chem. Soc.*, 2009, **131**, 8787.
15 (*a*) M. Murakami, K. Ohkubo and S. Fukuzumi, *Chem.–Eur. J.*, 2010, **16**, 7820; (*b*) M. Murakami, K. Ohkubo, T. Nanjo, K. Souma, N. Suzuki and S. Fukuzumi, *ChemPhysChem*, 2010, **11**, 2594.
16 L. Martín-Gomis, K. Ohkubo, F. Fernández-Lázaro, S. Fukuzumi and Á. Sastre-Santos, *J. Phys. Chem. C*, 2008, **112**, 17694.
17 S. Fukuzumi, H. Imahori, K. Okamoto, H. Yamada, M. Fujitsuka, O. Ito and D. M. Guldi, *J. Phys. Chem. A*, 2002, **106**, 1903.
18 Y. Kashiwagi, K. Ohkubo, J. A. McDonald, I. M. Blake, M. J. Crossley, Y. Araki, O. Ito, H. Imahori and S. Fukuzumi, *Org. Lett.*, 2003, **5**, 2719.
19 S. Fukuzumi, K. Ohkubo, W. E. Z. Ou, J. Shao, K. M. Kadish, J. A. Hutchison, K. P. Ghiggino, P. J. Sintic and M. J. Crossley, *J. Am. Chem. Soc.*, 2003, **125**, 14984.
20 K. Ohkubo, H. Kotani, J. Shao, Z. Ou, K. M. Kadish, G. Li, R. K. Pandey, M. Fujitsuka, O. Ito, H. Imahori and S. Fukuzumi, *Angew. Chem., Int. Ed.*, 2004, **43**, 853.
21 (*a*) S. Fukuzumi, M. Fujita, S. Noura, K. Ohkubo, T. Suenobu, Y. Araki and O. Ito, *J. Phys. Chem. A*, 2001, **105**, 1857; (*b*) H. Kitaguchi, K. Ohkubo, S. Ogo and S. Fukuzumi, *J. Phys. Chem. A*, 2006, **110**, 1718.
22 S. V. Frye, M. C. Johnson and N. L. Valvano, *J. Org. Chem.*, 1991, **56**, 3750.
23 L. Lu and S. A. Jenekhe, *Macromolecules*, 2001, **34**, 6249.
24 V. A. Kharlanov, W. Rettig, M. I. Knyazhansky and N. Makarova, *J. Photochem. Photobiol., A*, 1997, **103**, 45.

25 The energy of the singlet excited state of Qu^+ was determined from the absorption (λ_{max} = 316 nm) and emission maxima (λ_{max} = 397 nm).
26 (*a*) S. Fukuzumi and S. Noura, *J. Chem. Soc., Chem. Commun.*, 1994, 287; (*b*) S. Fukuzumi, M. Fujita, S. Noura, K. Ohkubo, T. Suenobu, Y. Araki and O. Ito, *J. Phys. Chem. A*, 2001, **105**, 1857.
27 (*a*) U. C. Yoon, S. L. Quillen, P. S. Mariano, R. Swanson, J. L. Stavinoha and E. Bay, *J. Am. Chem. Soc.*, 1983, **105**, 1204; (*b*) M. Nishimine, K. Ohkubo, T. Komori and S. Fukuzumi, *Chem. Commun.*, 2003, 1886.
28 (*a*) K. Ohkubo, K. Mizushima, R. Iwata, K. Souma, N. Suzuki and S. Fukuzumi, *Chem. Commun.*, 2010, **46**, 601; (*b*) K. Ohkubo, K. Mizushima, R. Iwata and S. Fukuzumi, *Chem. Sci.*, 2011, **2**, 715.
29 (*a*) S. Fukuzumi, T. Suenobu, M. Patz, T. Hirasaka, S. Itoh, M. Fujitsuka and O. Ito, *J. Am. Chem. Soc.*, 1998, **120**, 8060; (*b*) S. Fukuzumi, T. Suenobu, T. Hirasaka, N. Sakurada, R. Arakawa, M. Fujitsuka and O. Ito, *J. Phys. Chem. A*, 1999, **103**, 5935.
30 S. Fukuzumi, K. Ohkubo, T. Suenobu, K. Kato, M. Fujitsuka and O. Ito, *J. Am. Chem. Soc.*, 2001, **123**, 8459.
31 (*a*) L. Biczók and H. Linchitz, *J. Phys. Chem. A*, 2001, **105**, 11051; (*b*) J. K. Kochi, R. Rathore and P. L. Maguères, *J. Org. Chem.*, 2000, **65**, 6826.
32 The quantum yield of QuPh–NA" was determined by using the comparative method.[20]
33 (*a*) A. C. Benniston, A. Harriman, P. Li, J. P. Rostron and J. W. Verhoeven, *Chem. Commun.*, 2005, 2701; (*b*) A. C. Benniston, A. Harriman, P. Li, J. P. Rostron, H. J. van Ramesdonk, M. M. Groeneveld, H. Zhang and J. W. Verhoeven, *J. Am. Chem. Soc.*, 2005, **127**, 16054.
34 (*a*) S. Sekiguchi, Y. Kobori, K. Akiyama and S. Tero-Kubota, *J. Am. Chem. Soc.*, 1998, **120**, 1325; (*b*) Y. Kobori, T. Yago, K. Akiyama and S. Tero-Kubota, *J. Am. Chem. Soc.*, 2001, **123**, 9722; (*c*) Y. Kobori, Y. Shibano, T. Endo, H. Tsuji, H. Murai and K. Tamao, *J. Am. Chem. Soc.*, 2009, **131**, 1624.
35 K. Ohkubo, K. Suga, K. Morikawa and S. Fukuzumi, *J. Am. Chem. Soc.*, 2003, **125**, 12850.
36 (*a*) S. Fukuzumi, H. Imahori, K. Okamoto, H. Yamada, M. Fujitsuka, O. Ito and D. M. Guldi, *J. Phys. Chem. A*, 2002, **106**, 1903; (*b*) B. R. Arnold, A. W. Schill and P. V. Poloakov, *J. Phys. Chem. A*, 2001, **105**, 537.
37 (*a*) H. Kotani, T. Ono, K. Ohkubo and S. Fukuzumi, *Phys. Chem. Chem. Phys.*, 2007, **9**, 1487; (*b*) H. Kotani, R. Hanazaki, K. Ohkubo, Y. Yamada and S. Fukuzumi, *Chem.–Eur. J.*, 2011, **17**, 2777.
38 G. M. Sheldrick, *SHELX97, Programs for Crystal Structure Refinement*, University of Göttingen, Germany, 1997.
39 (*a*) A. J. Bard and L. R. Faulkner, In *Electrochemical Methods, Fundamental and Applications*, John Wiley & Sons, New York, 2001, chap. 10, pp. 368–416; (*b*) T. G. McCord and D. E. Smith, *Anal. Chem.*, 1969, **41**, 1423.
40 C. K. Mann and K. K. Barnes, *Electrochemical Reactions in Nonaqueous Systems*, Marcel Dekker, New York, 1990.
41 The WinSIM program is developed at the NIEHS by Duling (URL: http://www.niehs.nih.gov/research/resources/software/tools/index.cfm): D. R. Duling, *J. Magn. Reson., Ser. B*, 1994, **104**, 105.
42 (*a*) A. D. Becke, *J. Chem. Phys.*, 1993, **98**, 5648; (*b*) C. Lee, W. Yang and R. G. Parr, *Phys. Rev. B*, 1988, **37**, 785.
43 W. J. Hehre, L. Radom, P. V. R. Schleyer and J. A. Pople, *Ab Initio Molecular Orbital Theory*, Wiley, New York, 1986.

